PERGAMON

International Journal of Heat and Mass Transfer 44 (2001) 1711–1724

International Journal of HEAT and MASS TRANSFER

www.elsevier.com/locate/ijhmt

Experimental and numerical analysis of heat transfer phenomena in a sensor tube of a mass flow controller

Sung Jin Kim *, Seok Pil Jang

Department of Mechanical Engineering, Korea Advanced Institute of Science and Technology, 373-1 Kusong-dong, Yusong-gu, Taejon 305-701, South Korea

Received 26 April 2000; received in revised form 17 June 2000

Abstract

In the present work, the heat transfer phenomena in the sensor tube of a mass flow controller (MFC) are studied using both experimental and numerical methods. A numerical model is introduced to predict the temperature profile in the sensor tube as well as in the gas stream. In the numerical model, the conjugate heat transfer problem comprising the tube wall as well as the gas stream is analyzed to fully understand the heat transfer interaction between the sensor tube and the fluid stream, using a single domain approach. This numerical model is further verified by experimental investigation. In order to describe the transport of heat energy in both the flow region and the sensor tube, the Nusselt number distributions at the interface between the tube wall and the gas stream as well as heatlines are presented from the numerical solution. Through this study several assumptions frequently used by previous investigators for their analytical models have been shown to be either irrelevant or physically unrealistic.

1. Introduction

A mass flow controller (MFC) is widely used in many scientific and engineering processes for controlling the mass flow rate of a gas with an accuracy of 1% because the measurement and control of gas flow is critical in many applications such as engine and fuel cell tests, chemical reactions, and so on [1]. In particular, there are many semiconductor manufacturing processes where an MFC accurately delivers a stable and known mass flow rate of a gas to processing chambers. There are a variety of volumetric meters, such as orifice, rotary, swirl, ultra-sonic, and turbine. A volumetric meter measures a volume flow rate or velocity, but this must be corrected for temperature, pressure, viscosity and other variables in order to obtain the mass flow rate. However, an MFC can directly measure the mass flow rate without being corrected for temperature, pressure, viscosity, and other variables.

An MFC typically consists of a sensor tube, a bypass (main) tube, and a control valve. The sensor tube in an MFC is a long, slender stainless steel tube with heating wires and sensor windings. It is the most critical part of an MFC. The mass flow rate is sensed by heat transfer between a heated tube wall and a gas stream flowing in the sensor tube. There are several types of sensors, which vary according to the number of heaters and sensors used in the sensor tube. The typical sensor currently used in the semiconductor manufacturing and chemical processes consists of a single heater and two RTD sensors [2].

Heat transfer phenomena in the sensor tube are rather involved because heat generation in the heating wire, conduction in the tube wall, convection into the gas, and conduction loss through the insulation material are all happening simultaneously. Due to this complexity, many investigators have tried to describe the heat transfer phenomena in the sensor tube with a few simplifying assumptions. They are listed as follows:

Assumption I. The temperature of both ends of the sensor tube is kept constant regardless of the mass flow rate.

* Corresponding author. Tel.: +82-42-869-3043; fax: +82-42-869-3210.

E-mail address: sungkim@me.kaist.ac.kr (S.J. Kim).

0017-9310/01/$ - see front matter
PII: S0017-9310(00)00216-7

Nomenclature

B	bias error
C_p	specific heat
D	diameter of the sensor tube
f_e	interpolation factor
h	heat transfer coefficient
$\overline{h}$	average heat transfer coefficient
H	heatfunction
k	conductivity
L	axial length of the tube wall
L_e	entry length
$\dot{M}$	mass flow rate
N	data number
$\overline{Nu}$	average Nusselt number
p	pressure
P	precision error
q''	heat flux
$\dot{Q}$	heat source
r_{crit}	critical insulation radius
R_1	inner radius of the sensor tube
R_2	external radius of the sensor tube
R_3	radius of the insulation material
S_F	standard deviation
T'	true temperature
$\overline{T}$	mean temperature
T	temperature
u	axial velocity
U_m	mean velocity
U_T	uncertainty

Greek symbols

μ	gas viscosity
λ	degree of freedom

Subscripts/superscripts

down	downstream
down_e	end of the downstream
f	fluid
h	horizontal
H	harmonic mean
i	inlet
in	inner
ins	insulation material
m	mean
s	solid
sur	surrounding
up	upstream
v	vertical

Assumption II. The temperature of the tube wall is equal to the gas mean temperature in the sensor tube.

Assumption III. The Nusselt number is 4.36 at the interface between the tube wall and the gas stream in the entire sensor tube.

Recently Komiya et al. [3] suggested a one-dimensional analytic solution. Their work is based on adopting assumptions I and II in solving an energy equation in the sensor tube. Thus, the one-dimensional analytic solution proposed by Komiya et al. [3] is inherently limited to showing the temperature profile of the sensor tube wall only along the axial direction. In order to extend the work of Komiya et al. [3], Hinkle and Mariano [2] used a two-dimensional model to simulate the heat transfer phenomena in the sensor tube. They assumed that the flow in the sensor tube was fully developed both thermally and hydrodynamically. They also used assumption III to represent the heat transfer rate at the interface of the sensor tube, which is subject to a constant heat flux only at the central section of the tube wall. But assumption III is appropriate only when the entire circular tube is subject to a uniform surface heat flux. In addition, Hinkle and Mariano [2], just like Komiya et al. [3], applied assumption I as the boundary condition for their analytic solution.

Rudent and Navratil [4] presented an analytic model with the condition that the wall temperature was different from the gas mean temperature. Their analytic solution contains the Nusselt number, the heat loss coefficient, and the boundary conditions at the ends of the sensor tube. These factors have significant effects on the analytic solution and have to be determined experimentally. Instead, assumption III has frequently been used to calculate the analytic solution because it is difficult to obtain the Nusselt number distribution at the interface between the tube wall and the gas stream in the sensor tube by the experimental method. This in turn makes it difficult to estimate the gas temperature along the radial direction with the analytic solution proposed by Rudent and Navratil [4].

In the present study, the heat transfer phenomena in the sensor tube of the MFC are studied by using both experimental and numerical methods. A numerical model for a conjugate heat transfer problem comprising both the gas stream and the tube wall is introduced to estimate the temperature profile in the tube wall as well as in the gas stream. This numerical model is further verified by experimental results. The Nusselt number distribution between the tube wall and the gas stream is presented from the numerical solution. The net flow of heat energy is finally exhibited with heatlines obtained from numerical results in order to fully understand the heat transfer mechanism involved in the sensor tube of the MFC; this kind of information sheds light on an optimum design for the sensor tube. In addition, we intend to determine whether a few assumptions employed by previous investigators are physically realistic or not.

2. Mathematical formulation

2.1. Problem definition and model

The problem under consideration in this paper concerns the relation between the mass flow rate and the tube wall temperature difference across the heater. This relation is strongly related with heat transfer phenomena in the sensor tube of the MFC. The schematic diagram of a physical model is shown in Fig. 1. This model is called the single heater type, because it has only one heater. The axisymmetric coordinate is used to solve the problem. The direction of the gas flow is parallel with the x-axis. It is assumed that the velocity profile is fully developed while the temperature profile is just being developed in the flow region. The thermophysical properties of the gas as well as the tube wall are also assumed to be constant. A uniform heat flux is applied to the central part of the sensor tube where the heating wire is wound. As the MFC is typically calibrated with a nitrogen gas, we simulate the heat transfer phenomena in the sensor tube using nitrogen gas.

2.2. Governing equations

In order to analyze the heat transfer phenomena in the sensor tube of the MFC, momentum and energy equations for both the tube wall and the gas stream should be solved. As the full scale range of the gas flow that can be measured in the sensor tube is typically limited to low mass flow rates [2], the maximum range of the mass flow rate through the sensor tube in the present model is chosen to be 50 SCCM. The Reynolds number at the maximum mass flow rate is 62.16. Hence, the flow in the sensor tube can be safely assumed to be laminar.

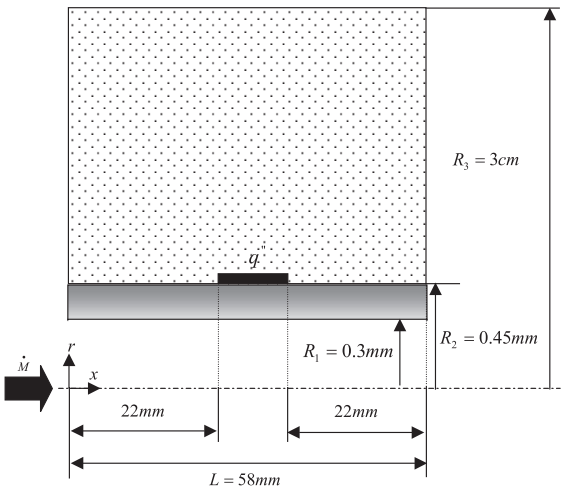

Fig. 1. Model of the sensor tube in the MFC: (a) physical model; (b) numerical model.

A reasonable approximation for the hydrodynamic entry length of the tube necessary for the development of the laminar velocity profile is calculated to be 1.82 mm [5]. Based on this entry length, the flow in the sensor tube can be considered as a fully developed Poiseuille flow in the circular tube. The velocity profile in the sensor tube is given as

$$u = 2U_{\text{mean}}\left(1 - \frac{r^2}{R_1^2}\right), \tag{1}$$

where U_{mean} and R_1 are mean velocity and the inner radius of the sensor tube.

The temperature field in the gas as well as in the tube wall and the insulation material is governed by the following energy equations:

$$\frac{1}{r}\frac{\partial}{\partial r}\left(k \cdot r\frac{\partial T}{\partial r}\right) + \frac{\partial}{\partial x}\left(k\frac{\partial T}{\partial x}\right) = \rho C_{\text{p}} u\frac{\partial T}{\partial x}, \tag{2}$$

where u, k, ρ, C_{p}, and T are axial velocity, thermal conductivity, gas density, specific heat of the gas, and temperature, respectively. Eq. (2) is solved subject to the following boundary conditions in the single computational domain comprising both solid (the tube wall and the insulation material) and fluid (gas) regions:

The boundary condition at $x = 0$ is

$$T_{\text{f}} = T_{\text{i}} \quad \text{in the flow region} \tag{3}$$

which implies that the inlet temperature of the gas flow is equal to the surrounding temperature. At the outflow boundary previous numerical models used $T_{\text{f}} = T_{\text{sur}}$ regardless of the mass flow rate [2,4]. However, this boundary condition is not physically realistic because the gas flow temperature is higher than the surrounding temperature due to convective heat transfer from the tube wall to the gas flow. In the present numerical model, the computational domain is extended in the axial direction so that the outflow boundary condition in the flow region can be assumed to be insulated, i.e.,

$$\left.\frac{\partial T}{\partial x}\right|_{x\to\infty} = 0. \tag{4}$$

Komiya et al. [3], Hinkle and Mariano [2], and Rudent and Navratil [4] incorporated a heat loss coefficient to account for heat losses which are transferred from the external surface of the tube wall to surroundings. They determined the loss coefficient using their experimental results. Their approach has a drawback in that their numerical model must always be accompanied by experimental investigation, and thus cannot be generally applied to other situations. To overcome this difficulty and to make the numerical model generally applicable, heat losses in the present model are considered to correspond to the existence of convection cooling at the outer surfaces of both the insulation material and the tube wall. This type of boundary condition is specified

via the heat transfer coefficient and the temperature of surroundings as proposed by Patankar [6]

$$-k\frac{\partial T_s}{\partial r} = \bar{h}_h(T_s - T_{sur}) \quad \text{at } r = R_3, \tag{5}$$

$$-k\frac{\partial T_s}{\partial x} = \bar{h}_v(T_s - T_{sur}) \quad \text{at } x = 0 \text{ and } x = L, \tag{6}$$

where $k, T_s, T_{sur}, \bar{h}_h(T_s)$ and $\bar{h}_v(T_s)$ are thermal conductivity, solid temperature, surrounding temperature, horizontal heat transfer coefficient, and vertical heat transfer coefficient, respectively. The boundary conditions (5) and (6) represent convective heat transfer to the ambient from the horizontal surface of the insulation material and the vertical surface of both ends of the tube wall and the insulation material, respectively. The heat loss coefficient, which is a function of the surface temperature at the insulation material, is obtained by Churchill and Chu's correlations (7)–(10) [7,8]

$$\overline{Nu}_h = \left\{ 0.6 + \frac{0.387 Ra_{D_{ins}}^{1/6}}{\left[1 + (0.559/Pr)^{9/16}\right]^{8/27}} \right\}^2 \quad \text{for } Ra_{D_{ins}} \leqslant 10^{12}, \tag{7}$$

$$\overline{h}_h(T) = \frac{k}{D_{ins}}\overline{Nu}_h, \tag{8}$$

$$\overline{Nu}_v = \left\{ 0.68 + \frac{0.607\ Ra_{L_{ins}}^{1/4}}{\left[1 + (0.492/Pr)^{9/16}\right]^{9/4}} \right\} \quad \text{for } Ra_{L_{ins}} \leqslant 10^{9}, \tag{9}$$

$$\overline{h}_v(T) = \frac{k}{L_{ins}}\overline{Nu}_v, \tag{10}$$

where $\overline{Nu}$, $\bar{h}$, Ra_D, Pr, k, D_{ins}, L_{ins} are average Nusselt number, average heat transfer coefficient, Rayleigh number, Prandtl number, conductivity and diameter and vertical length of the insulation material, respectively. The correlations proposed by Churchill and Chu provide the average Nusselt number and the average heat transfer coefficient over both the entire circumference and the vertical plate of an isothermal cylinder. In this work, it can be assumed from the measured temperature data that the surface of the insulation material is maintained at a constant temperature because the standard deviation of the temperature at the surface of the insulation material was 0.16 K. Since the Rayleigh number is 57,142, it is proper to use Churchill and Chu's correlation to obtain the average heat transfer coefficient.

In order to describe the transport of heat energy both in the flow region and in the tube wall region, we can define the heatfunction, $H(x, y)$ such that the net flow of energy is zero across each $H =$ constant [9,10]. Heatfunction is a combination of both thermal diffusion and enthalpy flow. From Eq. (2), the heatfunction is defined as

$$\frac{1}{r}\frac{\partial H}{\partial r} = \rho C_p u(T - T_i) - k\frac{\partial T}{\partial x}, \tag{11}$$

$$\frac{\partial H}{\partial x} = rk\frac{\partial T}{\partial x}, \tag{12}$$

where H, k, T, T_i, ρ, and C_p are heatfunction, thermal conductivity, temperature, inlet temperature, gas density, and specific heat of the gas, respectively. For a meaningful comparison of the heatlines of one flow with those of another flow, we set $H = 0$ at $r = 0$ because H is related to an arbitrary constant at $r = 0$. The heatfunction is obtained by integrating Eq. (11) both in the flow region and in the tube wall region.

2.3. Solution method

The governing equations are solved by the Control-Volume-based Finite Difference Method. The point successive over-relaxation (PSOR) method is utilized to reduce the time required for solving the governing energy equation [11].

The discontinuity of the thermal conductivity at the interface between the tube wall and the gas stream as well as at the interface between the tube wall and the insulation material is treated by placing a control surface at that location and utilizing the harmonic mean formulation for the thermal conductivity. The harmonic mean thermal conductivity is given by Patankar [6]

$$k_{H1} = \left(\frac{1 - f_e}{k_s} + \frac{f_e}{k_f}\right)^{-1} \quad \text{and} \quad k_{H2} = \left(\frac{1 - f_e}{k_{ins}} + \frac{f_e}{k_s}\right)^{-1}, \tag{13}$$

where $k_s, k_f, k_{ins}, f_e, k_{H1}$ and k_{H2} are conductivity of the tube wall, the gas stream and insulation material, interpolation factor, harmonic mean conductivity at the interface between the tube wall and gas stream and at the interface between the tube wall and the insulation material, respectively.

The energy equation, Eq. (2), is solved simultaneously both in the fluid part and the solid part by treating it as one computational domain. It is a so-called conjugate heat transfer problem. In a conjugate heat transfer problem, there are two physical mechanisms: one is conduction in the solid part, and the other is convection in the gas stream. The traditional conjugate coupling of conduction and convection heat transfer is usually accomplished by imposing at the interface the continuity of both the temperature and the heat flux. The finite-difference solution procedure adopted in this

work automatically satisfies the continuity of both the temperature and the heat flux at the interface between the insulation material and the tube wall as well as at the interface between the fluid part and the solid part [12], i.e.,

$$k_s \left.\frac{\partial T_s}{\partial r}\right|_{R_1^+} = k_f \left.\frac{\partial T_f}{\partial r}\right|_{R_1^-}, \quad k_s \left.\frac{\partial T_s}{\partial r}\right|_{R_2^+} = k_{ins} \left.\frac{\partial T_{ins}}{\partial r}\right|_{R_2^-}, \tag{14}$$

$$T_s|_{R_1^+} = T_f|_{R_1^-}, \quad T_s|_{R_2^+} = T_{ins}|_{R_2^-}, \tag{15}$$

where k_s, k_f, k_{ins}, T_s, T_f, T_{ins}, R_1, and R_2 are conductivity of the tube wall, the gas, and insulation material, tube wall temperature, gas temperature, insulation material temperature, inner radius and external radius of the sensor tube. When the rate of the maximum change in the temperature field is smaller than the specified maximum error, results are considered to be sufficiently converged. The convergence criterion is given as

$$\max \left|T^{n+1}(i,j) - T^n(i,j)\right| < 10^{-6}. \tag{16}$$

2.4. Grid test and benchmarking

A non-uniform grid was used both in the axial direction and in the radial direction in order to place a fine grid near the boundary and the interfaces. The grid dependence test was performed by changing the number of grid points. When the number of grid points is doubled in the radial direction from 55 and in the axial direction from 91, respectively, the maximum change of the temperature distribution is given as

$$\left|\frac{T - T^*}{T^*}\right|_{\max} \times 100 = 0.07\%, \tag{17}$$

where T, T^*, are temperature with a grid number of 91×55, and temperature with the number of grid points doubled. So, the grid used in the model is 91 in the axial direction, and 55 in the radial direction.

Before the code was applied to analyze the heat transfer phenomena in the sensor tube of the MFC, results for the temperature profiles and heatlines were validated by solving the benchmarking problem. Heat transfer to a circular tube flow with a conducting solid wall is solved with the code for benchmarking. It is assumed that the flow is thermally developing and hydrodynamic fully developed and that the solid part has a very high thermal conductivity. This is because the analytic solution exists for convective flow in a circular tube maintained at a constant temperature. The temperature profiles obtained from both the numerical and exact solutions are compared in Fig. 2. The maximum error between the numerical solution and the exact solution is 0.3% of the full scale temperature.

3. Experimental apparatus and technique

3.1. Experimental apparatus and method

The experimental arrangement is shown in Fig. 3(a). In order to analyze the heat transfer phenomena in the sensor tube of the MFC experimentally, we use nitrogen gas in this experiment because the MFC currently used in the semiconductor fabrication processes is calibrated with nitrogen gas. The concentration of nitrogen gas is 99.9993%. The nitrogen gas flows from a pressure tank through a pressure regulator, a metering valve, and the standard MFC to the sensor tube. In order to simulate the conditions encountered in the semiconductor manufacturing processes, we use a stainless steel tube

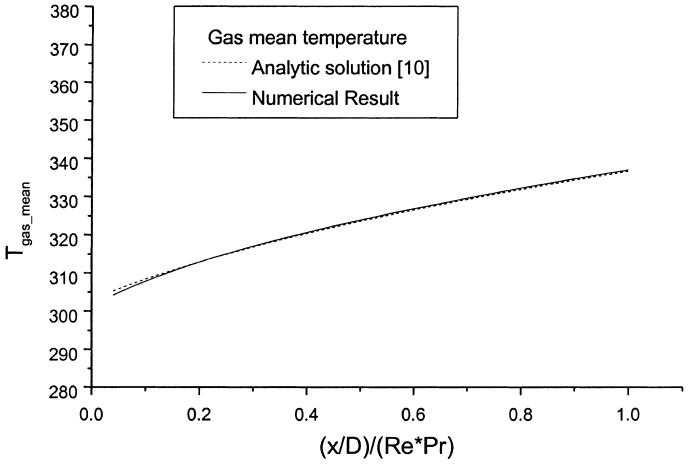

Fig. 2. Benchmarking: comparison between numerical solution and analytic solution.

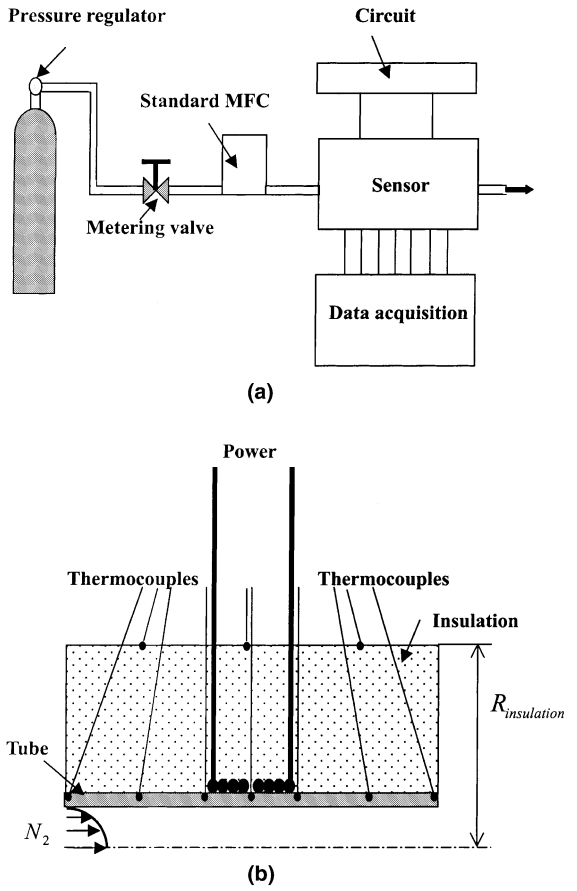

Fig. 3. Experimental apparatus: (a) experimental arrangement; (b) experimental prototype of the sensor tube.

processed by electropolishing. The electropolished tube is utilized for all pipes. The diameter of the tube is 6.35 mm. Both the pressure regulator and the metering valve are used to maintain constant pressure.

A standard MFC, model UFC-8160, provided by UNIT Instruments Incorporated, is used to measure and control the mass flow rate of the nitrogen gas in the current experiment. Its accuracy and repeatability are, respectively, ±1% and ±0.15% of the full scale. The full scale range in the MFC is 100 SCCM. The circuit is powered by an automatically controlled DC power supply manufactured by Hewlett Packard. Its accuracy is ±0.1% of the full scale range. The sensor tube is heated with a power of 0.508 W. The experimental prototype is shown in Fig. 3(b). The sensor tube is made of the stainless steel tube 316 L, which has an external diameter of 0.9 mm, an inner diameter of 0.6 mm and a length of 58 mm. The heating wire is an alloy of 60% nickel, 16% chromium, and an accepted material for heating devices operating up to 1283 K, and has a nominal temperature coefficient of a resistance which is 0.00015 Ω/°C. The diameter of the heating wire used in the experiment is 0.254 mm. The insulation material is made of glass fibers, of which the conductivity is 0.038 (W/m K). The radius of the insulation material is 0.03 m. The critical insulation thickness is calculated to 0.014 m [13]. From these results, it is validated that the insulation thickness used in the sensor tube is about two times larger than the critical insulation thickness.

The goal of the experimental investigation is to measure the temperature on the tube wall at as many locations as possible without altering the thermal properties of the surface. Seven thermocouples are instrumented on the outer surface of the sensor tube and three thermocouples on the outer surface of the insulation. The main disadvantage of using the thermocouples is that the thermocouple wire is thermally conductive and falsifies the temperature at the measuring point. However, this error can be minimized by using a K-type miniature thermocouple wire with a diameter of 0.0254 mm, which is provided by OMEGA Engineering. All thermocouple wires run parallel to the isothermal line in the tube wall. Thus, the error due to heat conduction through the thermocouple wires is minimized. The rationale of the positioning of the thermocouples, shown in Fig. 3(b), is to be able to observe the temperature profile at the surface of the sensor tube as well as at the surface of the insulation material. Temperature profiles on the sensor tube are measured at mass flow rates ranging from 10 to 50 SCCM with an increment of 10 SCCM.

3.2. Uncertainty analysis

The uncertainty of the temperature measurement results from measurement errors produced by electrical noise, etc. The measurement error, which consists of bias error and precision error, is divided into calibration errors, data acquisition errors, and data reduction errors.

In the experiment, we consider both the bias error from the thermocouples and the precision error from the repeatability of the data measured by the thermocouple in obtaining the uncertainty of the temperature measurement. The bias error of the data acquisition is disregarded because it is very small. The uncertainty evaluation is performed in accordance with a 95% confidence interval [14]

$$U_T = [B^2 + (t_{\lambda,95\%}P)^2]^{1/2}, \tag{18}$$

where U_T, B, and $t_{\lambda,95\%}P$ are measurement uncertainty, bias error, and estimate of the precision error in the repeated temperature measurement at 95% confidence. In addition, λ is the degree of freedom:

$$\lambda = N - 1, \tag{19}$$

where N is a data number. This method for the estimation of the uncertainty parallels the uncertainty

standard approved by professional societies as well as by the National Institute of Standards and Technology (NIST) in the United States. The bias error produced by the thermocouple is ±2.2°C, proposed by American National Standard Institute (ANSI). The precision error is determined by

$$P = \frac{S_F}{N^{1/2}}, \tag{20}$$

$$S_F = \sqrt{\frac{1}{N}\sum_{i=1}^{N}(T_i - \overline{T})^2}, \tag{21}$$

where P, S_F, N, and $(T_i - \overline{T})$ are precision error, standard deviation, data number, and deviation of T_i. The true value is given as

$$T' = \overline{T} \pm U_T \ (95\%), \tag{22}$$

where $T', \overline{T}$, and U_T are true temperature, mean temperature measured, and uncertainty of the temperature measurement.

4. Results and discussion

4.1. Comparison between numerical results and experimental results

In the present work, the emphasis is on analyzing the heat transfer phenomena in the sensor tube and presenting an appropriate numerical model. In order to verify the numerical model, we compare the numerical results for the surface temperature distribution on the sensor tube with experimental results. Fig. 4 shows the comparison between experimental and numerical results for the tube wall temperature profiles at the various mass flow rates. The experimental data are represented by circular symbols with uncertainty bars and the results of the simulation by solid lines. The simulation is run at mass flow rates ranging from 10 to 50 SCCM with an increment of 10 SCCM. In Fig. 4, the numerical results are shown to agree well with the experimental results. The tube wall temperature profile is symmetric without gas flow, but it shifts along the axial direction depending on the mass flow rate. The higher the mass flow rate is, the lower the surface temperature is at the upstream section, and the higher the surface temperature is at the downstream section. As a result, the temperature difference between the downstream section and the upstream section on the sensor tube is proportional to the mass flow rate. This phenomenon is the basic principle of the sensor tube of the MFC.

From the experimental and numerical results in Fig. 4, it can be assumed that the temperatures of both the gas and the tube wall at the end of the sensor tube are almost equal to the surrounding temperature (assumption I), when the mass flow rate of the nitrogen gas is below 10 SCCM, as Komiya et al. [3] and Hinkle and Mariano [2] have done. However, when the mass flow rate of the nitrogen gas exceeds 10 SCCM, assumption I used in [2,3] is no longer appropriate. The reason is that the heat transferred from the tube wall to the gas at the upstream section is transferred back to the downstream section by convection. Hence, the tube wall temperature is increased with the mass flow rate at the end of the downstream section of the sensor tube, as shown in Fig. 5.

4.2. Analysis of the heat transfer phenomena in the sensor tube

When the nitrogen gas flows through the sensor tube at a mass flow rate of 30 SCCM, the temperature profiles at the heating section along the radial direction are shown in Fig. 6. It is shown that the temperature gradient is changed from positive to negative at the heating section. It is estimated that the heat supplied at the heating section is transferred along the axial tube wall by conduction. Then, the heat is transferred from the wall to the gas stream at the upstream section; and on the contrary, from the gas to the wall at the downstream section by the convection.

The relation between the temperatures at both the upstream and downstream sections and the mass flow rate is shown in Fig. 7. The higher the mass flow rate is, the higher the temperature difference between the wall and the gas stream is at the downstream section as well as at the upstream section.

Fig. 8 clearly shows that the wall temperature becomes different from the gas mean temperature as the mass flow rate is increased. The difference between the gas mean temperature and the wall temperature increases with the mass flow rate. Thus, when the nitrogen gas flows through the sensor tube, assumption II, as proposed by Komiya et al. [3], that the gas mean temperature is equal to the wall temperature, would not be appropriate in analyzing the heat transfer phenomena in the sensor tube. On the other hand, the assumption that the gas mean temperature is different from the wall temperature, as adopted by Hinkle and Mariano [2] and Rudent and Navratil [4], is reasonable.

Numerical and experimental results from the present study are compared with results from the one-dimensional analytic solution presented by Komiya et al. [3]. When the mass flow rate is 10 SCCM, the results of Komiya et al. have accuracy similar to the present numerical results compared to experimental data. On the other hand, when the mass flow rate goes over 10 SCCM, they are quite different, because the one-dimensional analytic solution calculated by Komiya et al.

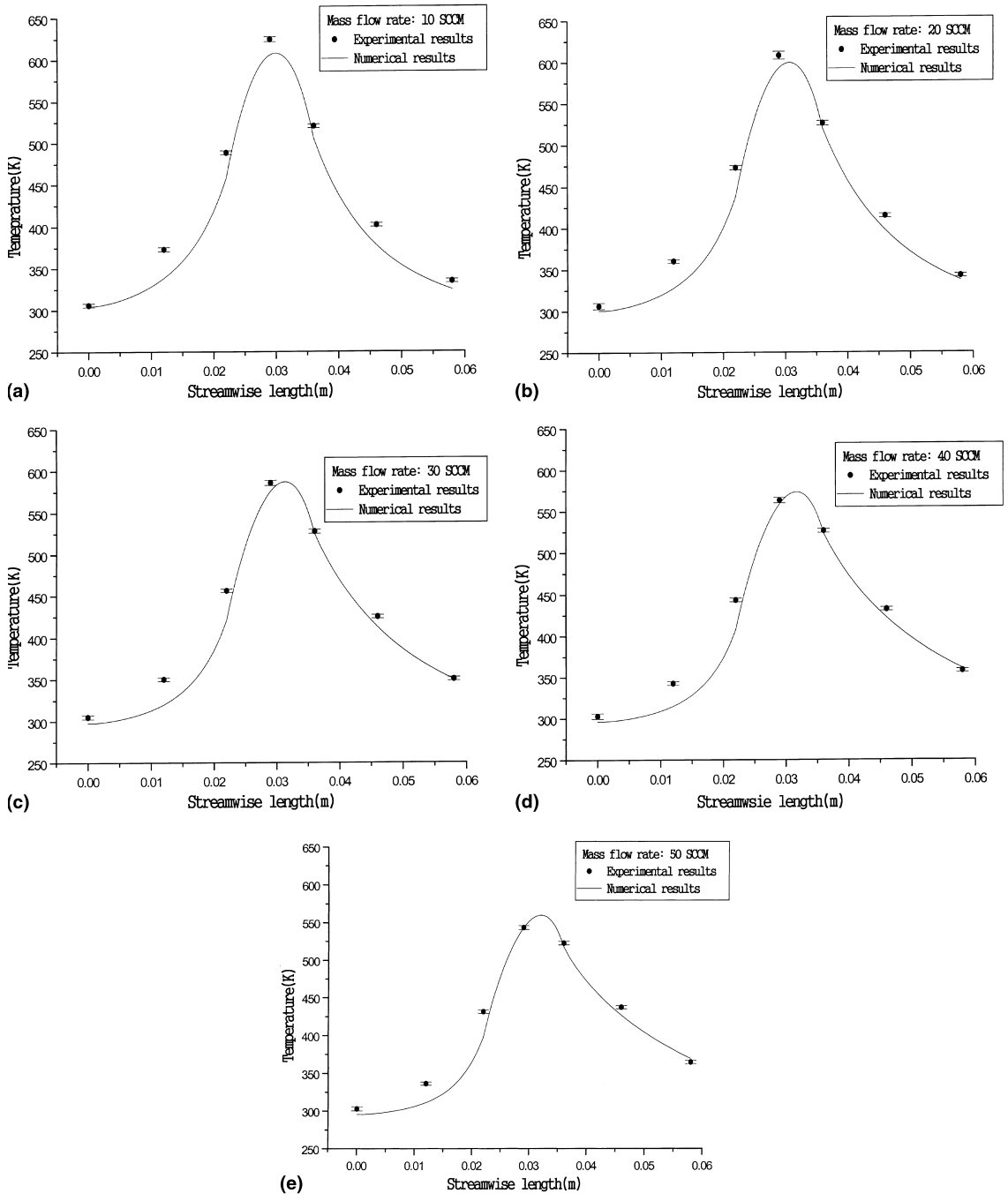

Fig. 4. Comparison between experimental and numerical tube wall temperature profile: (a) 10 SCCM; (b) 20 SCCM; (c) 30 SCCM; (d) 40 SCCM; (e) 50 SCCM.

[3] uses assumptions I and II. The fact that Komiya et al. [3] neglected the heat transfer along the radial direction in turn leads further to erroneous results.

In order to describe the transport of heat energy, the Nusselt number distribution as well as the heatlines are calculated with the numerical method. The Nusselt number, which is a dimensionless temperature gradient at the interface between the tube and the gas stream, is deduced from

$$Nu = \frac{hD_{\mathrm{in}}}{k_{\mathrm{f}}} = \frac{1}{T_{\mathrm{s}} - T_{\mathrm{m}}} \frac{\partial T}{\partial r}\bigg|_{r=R_1} D_{\mathrm{in}}, \tag{23}$$

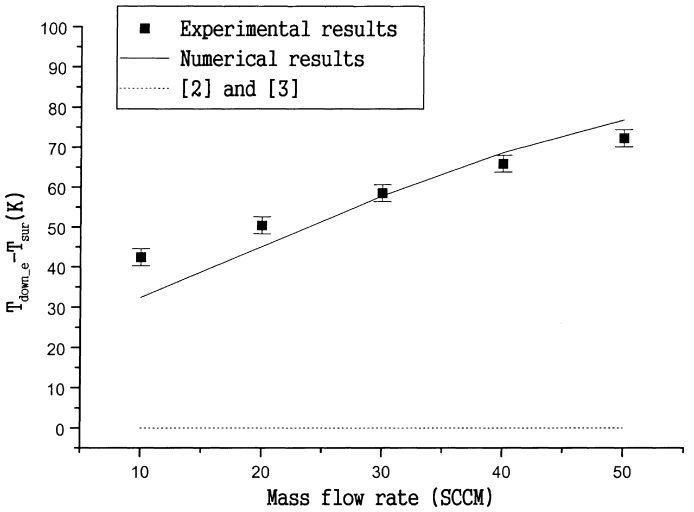

Fig. 5. Relation between the temperature difference at the end of the downstream section and the mass flow rate.

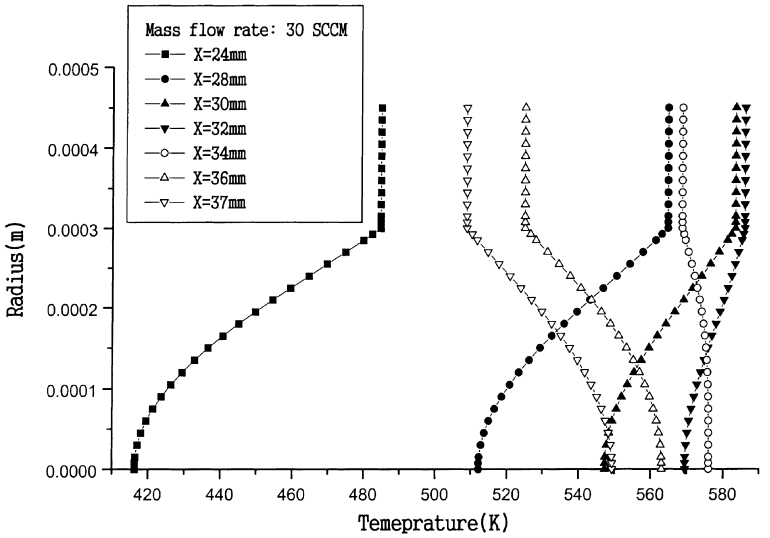

Fig. 6. Temperature profiles along the radial direction with 30 SCCM at the heating section.

where h, D_{in}, k_f, T_s, T_m, and R_1 are heat transfer coefficient at the solid–gas interface, inner diameter of the sensor tube, gas conductivity, wall temperature at the interface, gas mean temperature, and inner radius of the sensor tube, respectively. Fig. 9 shows the Nusselt number distributions at the solid–gas interface in the sensor tube. At the point near the end of the heating section, the temperature gradient is changed from positive to negative, where the Nusselt number is divergent. In the other part of the tube the Nusselt number is kept nearly constant at about 4.5 regardless of the mass flow rate. The Nusselt number of 4.36 (assumption III) used by Hinkle and Mariano [2] and Rudent and Navratil [4] is similar to the Nusselt number calculated by the present model at both the upstream section and the downstream section. However, near the end of the heating section including the singular point, assumption III cannot be used.

Finally, heatlines are shown in Fig. 10 in order to better describe the net flow of the heat energy in the sensor tube comprising both the tube wall and the gas stream. Heatlines, H = constant, are locally parallel to the direction of net energy flow through both the convection field and conduction field [9,10]. In addition,

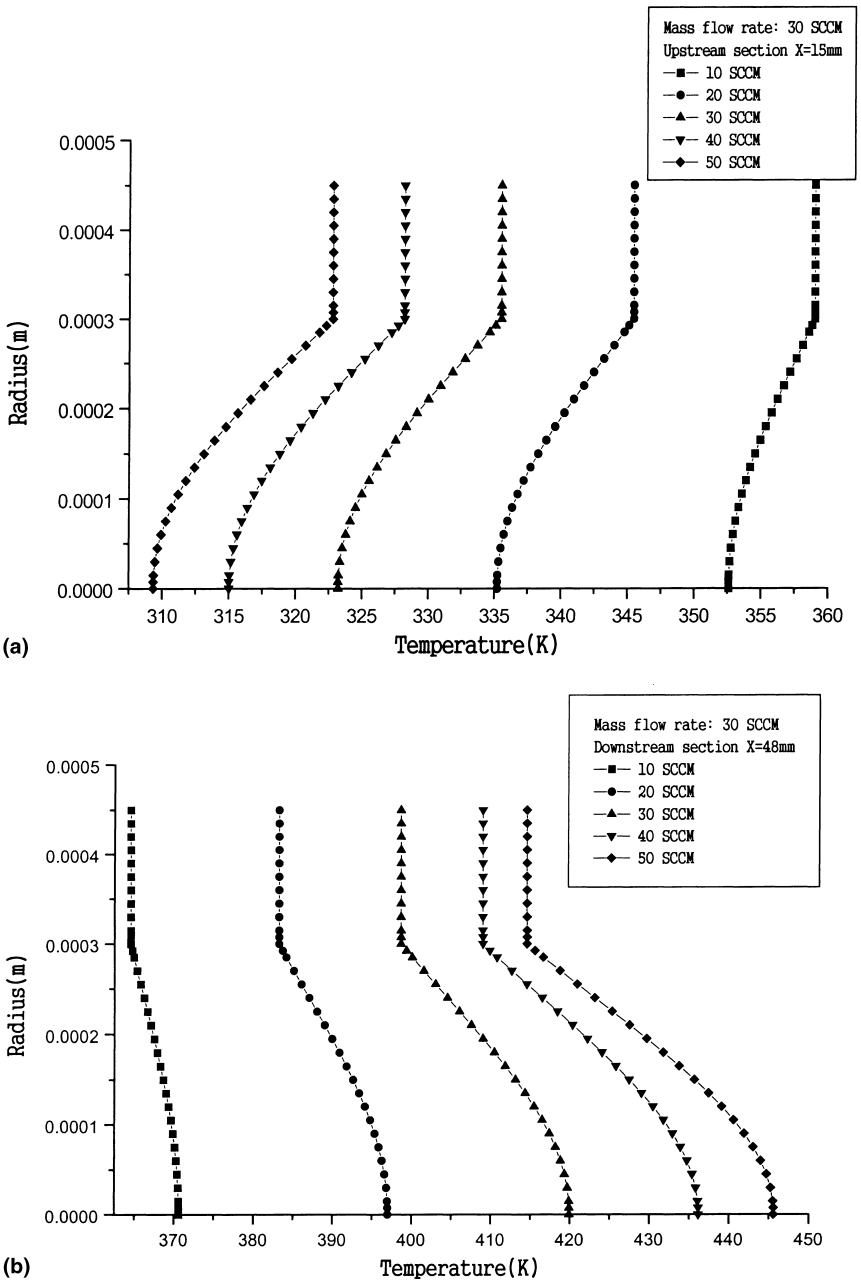

Fig. 7. Relation between the temperature profiles along the radial direction and the mass flow rate: (a) upstream section ($x = 15$ mm); (b) downstream section ($x = 48$ mm).

the narrower the spacing between two adjacent heatlines is, the higher is the heat energy transferred between the heatlines. In Fig. 10, the tube wall starts from 0.3 to 0.45 mm along the radial direction and the remaining part is gas stream. It is clearly shown by these heatlines that heat generated by the heating section is transferred along the axial tube wall by conduction. It is then transferred from the wall to the gas stream at the upstream section and from the gas stream to the wall at the downstream section by convection. At the upstream section, the higher the mass flow rate is, the higher is the heat energy transferred from the tube wall to the gas stream. Thus, the tube wall temperature at the upstream section is decreased with the mass flow rate. On the other hand, at the downstream section, the higher the mass flow rate, the higher the heat energy transferred

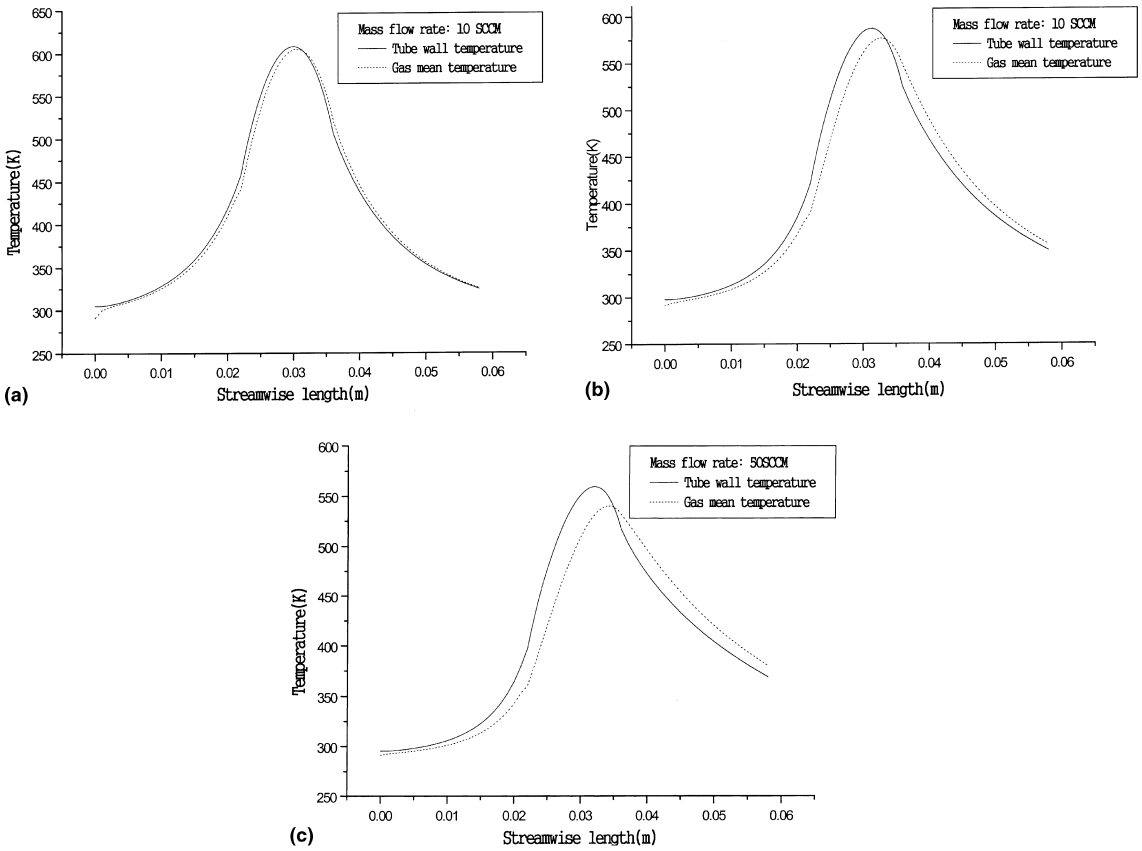

Fig. 8. Comparison between the wall temperature and the gas mean temperature: (a) 10 SCCM; (b) 30 SCCM; (c) 50 SCCM.

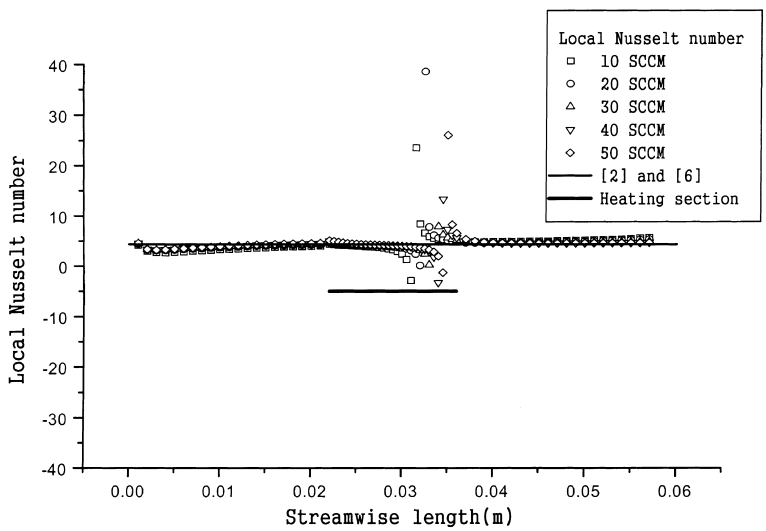

Fig. 9. Local Nusselt number at the interface between the tube wall and the gas stream.

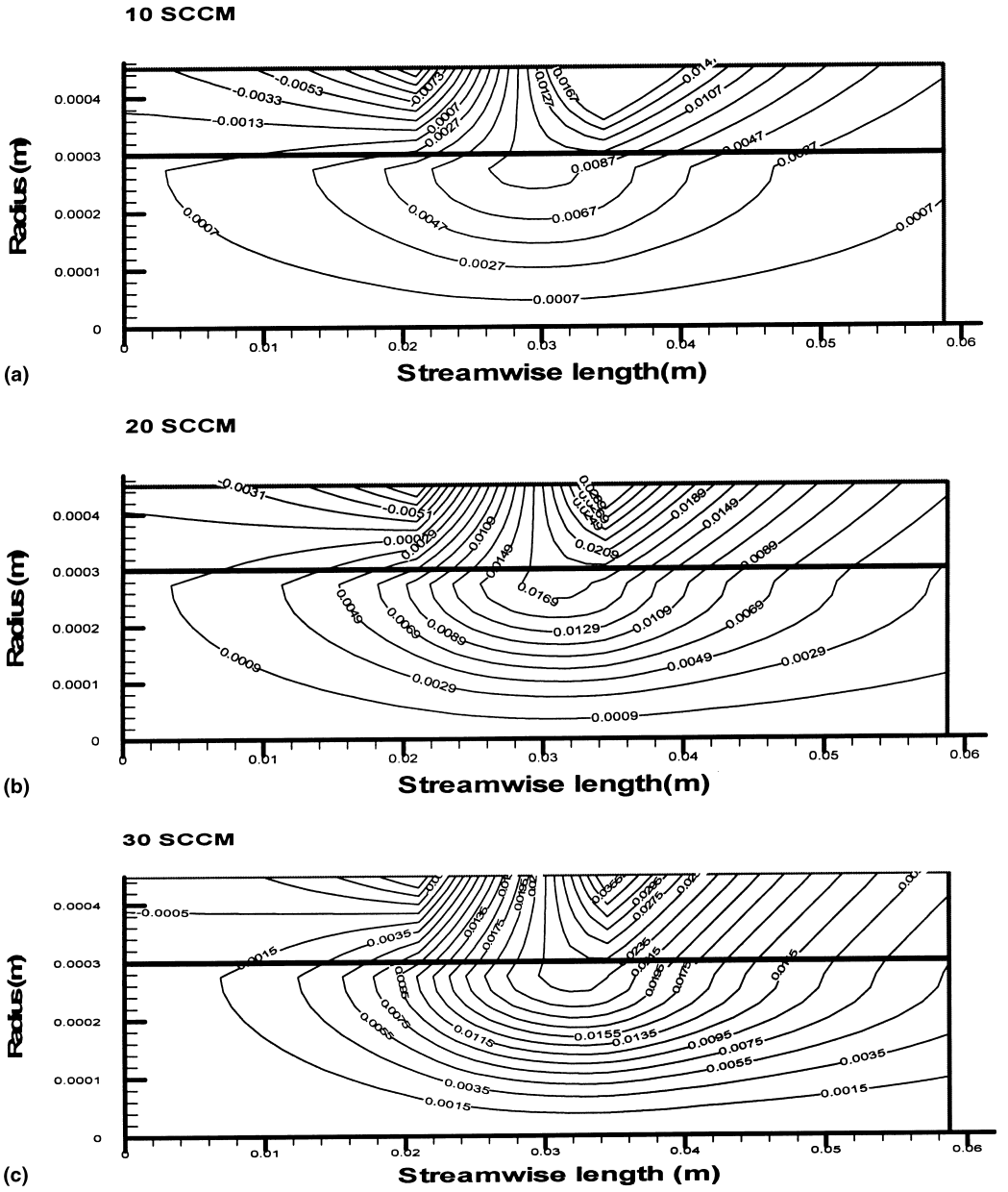

Fig. 10. Heatlines in the sensor tube: (a) 10 SCCM; (b) 20 SCCM; (c) 30 SCCM; (d) 40 SCCM; (d) 50 SCCM.

from the gas stream to the tube wall. Therefore, the tube wall temperature at the downstream section is increased with the mass flow rate.

5. Conclusion

In this work, the heat transfer phenomena that arise when nitrogen gas flows through the sensor tube of an MFC are studied using both experimental and numerical methods. A numerical model is introduced to estimate the temperature profile in the sensor tube as well as in the gas stream. The numerical model is further verified by experimental results. In order to explain the transport of heat energy both in the flow region as well as in the tube wall, not only the Nusselt number distributions at the interface between the tube wall and the gas stream, but also heatlines which show the transport of heat energy are presented by the numerical solutions.

In the sensor tube, the physical mechanism regarding the transport of heat energy is shown to be that the heat generated by the heating wire is transferred along the

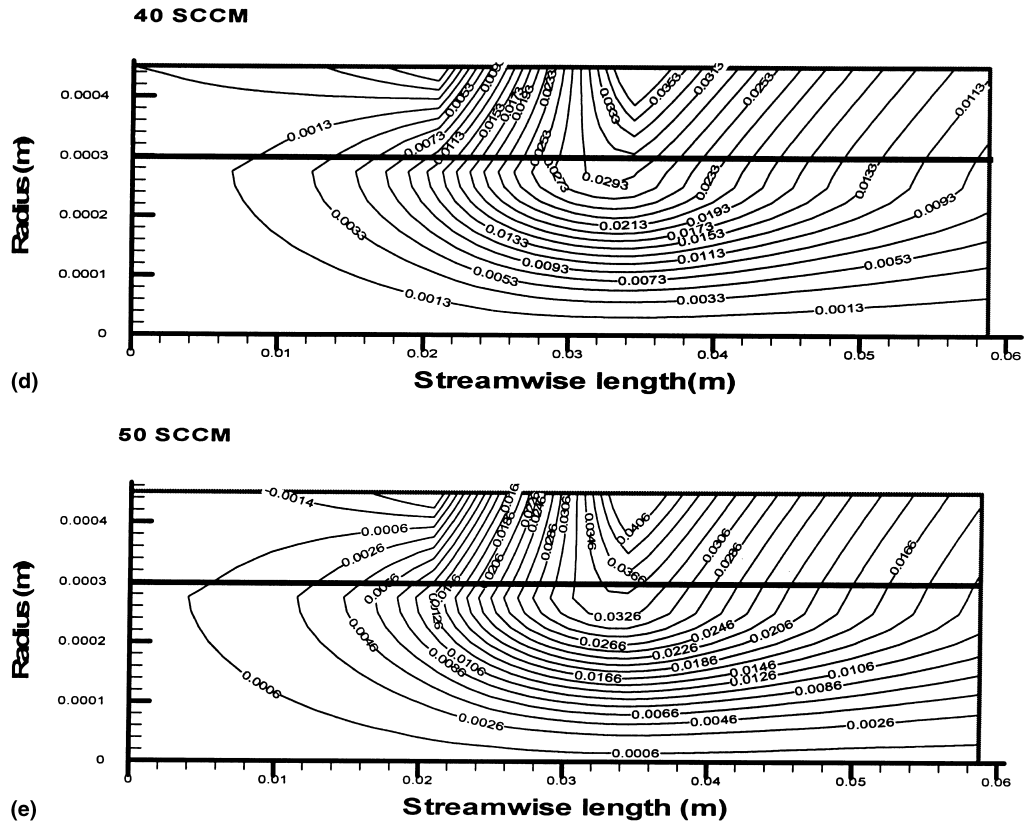

Fig. 10 (*continued*)

axial tube wall by conduction. It is then transferred from the tube wall to the gas stream at the upstream section and reversely, from the gas stream to the tube wall at the downstream section by convection. For a mass flow rate below 50 SCCM, the higher the mass flow rate, the higher the heat transferred by this mechanism. Therefore, the temperature difference between the upstream section and the downstream section is increased with the mass flow rate.

From the experimental and numerical results, it can be seen that the temperature of both the gas and the tube wall at the end of the sensor tube is similar to the surrounding temperature when the mass flow rate of the nitrogen gas is below 10 SCCM. Therefore, assumption I proposed by Komiya et al. [3] and Hinkle and Mariano [4] is reasonable at small mass flow rates. But when the mass flow rate of the nitrogen gas exceeds 10 SCCM, assumption I proposed by them can no longer be used.

Assumption II, that the surface temperature on the sensor tube is equal to the gas mean temperature, is shown to be inappropriate because the heat transfer along the radial direction is produced at the sensor tube by the temperature difference between the tube wall and the gas.

The Nusselt number of 4.36 (assumption III) used by Hinkle and Mariano [2] and Rudent and Navaratil [4] is appropriate both at the upstream section and at the downstream section, because the Nusselt number of 4.5 at the interface between the tube wall and the gas stream is shown to be kept nearly constant regardless of the mass flow rate from the numerical results. But at the heating section, where the temperature gradient changes from positive to negative, assumption III is no longer valid. The Nusselt number is divergent at the singular point.

Finally, the net flow of heat energy is exhibited with heatlines obtained from numerical results in order to fully understand the heat transfer mechanism involved in the sensor tube of the MFC, information which sheds light toward an optimum design of the sensor tube.

Acknowledgements

This work was supported by KOSEF (Korea Science and Engineering Foundation) and KISTEP (Korea Institute of Science & Technology Evaluation and Planning) under grant number 2-578 through the National Research Lab Program.

References

[1] J.M. Benson, W.C. Baker, E. Easter, Thermal mass flowmeter, Instr. Control Syst. 43 (1970) 85–87.
[2] L.D. Hinkle, C.F. Mariano, Toward understanding the fundamental mechanisms and properties of the thermal mass flow controller, J. Vac. Sci. Technol. 9 (1991) 2043–2047.
[3] K. Komiya, F. Higuchi, K. Ohtani, Characteristics of a thermal gas flowmeter, Rev. Sci. Instr. 59 (3) (1988) 477–479.
[4] P. Rudent, P. Navratil, Design of a new sensor for mass flow controller using thin-film technology based on an analytic thermal model, J. Vac. Sci. Technol. 16 (1998) 3559–3563.
[5] W.M. Kays, M.E. Crawford, Convective Heat and Mass Transfer, third ed., McGraw-Hill, New York, 1993 (Chapter 7).
[6] S.V. Patankar, Numerical Heat Transfer and Fluid Flow, first ed., Taylor & Francis, London, 1980 (Chapter 4).
[7] S.W. Churchill, H.H.S. Chu, Correlating equations for laminar and turbulent convection from a horizontal cylinder, Int. J. Heat Mass Transfer 18 (1975) 1049–1053.
[8] S.W. Churchill, H.H.S. Chu, Correlating equations for laminar and turbulent free convection from a vertical plate, Int. J. Heat Mass Transfer 18 (1975) 1323–1329.
[9] A. Bejan, Convection Heat Transfer, second ed., Wiley, New York, 1995 (Chapter 1).
[10] S. Kimura, A. Bejan, Visualization of convective heat transfer, ASME J. Heat Transfer 105 (1983) 916–919.
[11] K.A. Hoffmann, S.T. Chiang, Computational Fluid Dynamics for Engineers, first ed., A Publication of Engineering Education System 1, Wichita, Kansas, 1993 (Chapter 5).
[12] K. Vafai, S.J. Kim, Analysis of surface enhancement by a porous substrate, ASME J. Heat Transfer 112 (1990) 700–706.
[13] J.P. Holman, Heat Transfer, seventh ed., McGraw-Hill, New York, 1990 (Chapter 2).
[14] S.F. Richard, E.B. Donald, Theory and Design for Mechanical Measurements, second ed., Wiley, New York, 1995 (Chapter 5).